Supporting Information

Pt-Ni@PC900 Hybrid derived from layered structure Cd-MOF for fuel cell ORR activity

Muhammad Nadeem[a,b,d†], Ghulam Yasin[b†], Muhammad Arif[b] Moazzam H. Bhatti[a], Koray Sayin[c], Mazhar Mehmood[d], Uzma Yunus[a], Shoaib Mehboob[d], Imtiaz Ahmed[a] and Ulrich Flörke[b]*

[a] Department of Chemistry, Allama Iqbal Open University, Islamabad, Pakistan

[b] State Key Laboratory of Chemical Resource Engineering, Institute of Science, and College of Energy, Beijing University of Chemical Technology, Beijing 100029, P. R. China.

[c] *Department of Chemistry, Institute of Science, Cumhuriyet University 58140 Sivas – Turkey*

[d] *National Center for Nanotechnology, Department of Metallurgy and Materials Engineering, Pakistan Institute of Engineering and Applied Sciences (PIEAS), Nilore 45650, Islamabad, Pakistan*

[e] *Anorganische und Analytische Chemie, Fakultät für Naturwissenschaften, Universität Paderborn, Warburgerstrasse 100, D-33098 Paderborn, Germany*

E-mail of corresponding Author:
* moazzamhussain_b@yahoo.com (M.H. Bhatti).
†These authors contributed to this paper equally.

Computational Method

The quantum chemical calculations of Cd-MOF are performed by Gaussian programs. [1, 2] The hybrid density functional theory was used by utilizing B3LYP with LANL2DZ basis set. [3, 4] The scaling factor of 0.961 was used for IR frequencies to calculate anharmonic frequencies. UV-VIS spectrum of related compound was calculated through TD-B3LYP/LANL2DZ level in gas phase, DMSO, ethanol and water. Conductor polarized continuum model (C-PCM) was used in calculation of solute-solvent interactions. Additionally, some quantum chemical parameters which are static dipole moment (μ), average linear polarizability (α), anisotropic polarizability (Δα), the first hyperpolarizability (β) and optical softness (σ_O) were calculated via Eq. (1) – (5). [5, 6]

$$\boldsymbol{\mu} = \sqrt{\boldsymbol{\mu_x^2} + \boldsymbol{\mu_y^2} + \boldsymbol{\mu_z^2}} \quad (1)$$

$$\boldsymbol{\alpha} = \frac{\mathbf{1}}{\mathbf{3}}(\boldsymbol{\alpha_{xx}} + \boldsymbol{\alpha_{yy}} + \boldsymbol{\alpha_{zz}}) \quad (2)$$

$$\Delta\boldsymbol{\alpha} = \frac{\mathbf{1}}{\sqrt{2}}[(\boldsymbol{\alpha_{xx}} - \boldsymbol{\alpha_{yy}})^{\mathbf{2}} + (\boldsymbol{\alpha_{yy}} - \boldsymbol{\alpha_{zz}})^{\mathbf{2}} + (\boldsymbol{\alpha_{zz}} - \boldsymbol{\alpha_{xx}})^{\mathbf{2}} + \mathbf{6}\boldsymbol{\alpha_{xz}^2} + \mathbf{6}\boldsymbol{\alpha_{xy}^2} + \mathbf{6}\boldsymbol{\alpha_{yz}^2}]^{\mathbf{1/2}} \quad (3)$$

$$\boldsymbol{\beta} = [(\boldsymbol{\beta_{xxx}} + \boldsymbol{\beta_{xyy}} + \boldsymbol{\beta_{xzz}})^{\mathbf{2}} + (\boldsymbol{\beta_{yyy}} + \boldsymbol{\beta_{yxx}} + \boldsymbol{\beta_{yzz}})^{\mathbf{2}} + (\boldsymbol{\beta_{zzz}} + \boldsymbol{\beta_{zxx}} + \boldsymbol{\beta_{zyy}})^{\mathbf{2}}]^{\mathbf{1/2}} \quad (4)$$

$$\boldsymbol{\sigma_o} = \frac{\mathbf{1}}{\boldsymbol{E_{GAP}}} \quad (5)$$

General Characterization Techniques

The single crystal of the Cd-MOF was analysed by the Bruker SMART CCD area-detector diffractometer through intensity collection data. The measurements were carried out at temperature 130K by utilizing monochromated radiation of wavelength 7.1073 nm. The structure has been figured out after acquiring data from equivalents reflections (after the application of semi empirical absorption corrections) with SHELXLS-97 and the atomic model refined against $|F|^2$. [7] All atoms excluding hydrogen had been

elaborated an-isotropically. The isotropic displacement measurements like $U_{iso}(H) = 1.2U_{eq}(C/O)$ and C-H 0.95-0.98 Å have been utilized to find out hydrogen atoms riding on the parent atoms from difference Fourier maps. The Nicolet iS 10 FTIR Spectrophotometer (4000-400 cm^{-1}) was utilized for FTIR spectra (KBr-discs) of compounds i.e H_2BDC and Cd-MOF. The UV-1800 Shimadzu spectrophotometer was used for UV-Vis spectra of compounds. The BET surface area and pore volume curves for Cd-MOF have been calculated through Autosorb iQ3 gas sorption analyzer by utilization of liquid nitrogen bath at 77K. The Cd-MOF was activated at 100 °C for 12 h under vacuum. The Femto Fiber Pro laser system from TOPTICA Photonics was employed for tera hertz measurements. The details of measurement can be found as reported by Nadeem et al. [8, 9]

Measurements for ORR

ORR measurements were performed through Autolab PGSTAT302N (Metrohm) work station which was coupled with the rotating electrode. The measurement was performed by the electrolytic cell which comprises three electrodes present in 0.1 **M** KOH electrolyte i.e. Ag/AgCl as reference electrode, Pt wire as counter electrode, Rotating ring disk electrode (RRDE) and Rotating disk electrode (RDE) both these were used as working electrodes. The scan rate used for linear sweep voltammograms was 5 mVs^{-1}. The onset potentials (E_{onset}) were determined by taking the assumption that the potential at which the current density attains 1% of limiting current density. The halfwave potential is the potential measured where the current density becomes half of the limiting current density.

The ink of the Pt-Ni@PC900 and 20%Pt/C was prepared by dispersing 5mg of each compound separately in 1 ml H_2O, then 25 µL of 5%Nafion D-521 dispersion (Alfa Aesar) along with 250

μL of isopropanol was added in the dispersion. The whole mixture was sonicated for 3 hours. The precise amount of ink (20 μL) was applied onto a glassy carbon of RRDE and RDE, allowed to dry in air, giving a catalyst loading of 316 μg cm^{-2} for all samples. The O_2 saturated electrolyte was prepared by purging O_2 (99.999 %) into the electrolyte solution for 30 minutes. For comparison, CV measurements were also performed in an N_2 (99.99%)-saturated electrolyte. For RDE measurements, the working electrode was scanned at a rate of 5 mVs^{-1} at various rotation speeds (400, 625, 900, 1225, 1600 and 2025 rpm). The Koutecky-Levich equation is as under.

$$\frac{1}{J} = \frac{1}{J_K} + \frac{1}{J_d} = \frac{1}{J_K} + \frac{1}{A * \sqrt{\omega}}, A = 0.2nFC_O D^{2/3} \nu^{-1/6}$$

Where J = observed current density
J_K = kinetic current density
J_d = diffusion current density

The other parameters are ω used for the rotation of electrode in rpm, *F* is denoted as Faraday constant (96485 C mol^{-1}), C_0 is for bulk concentration of O_2 (1.26×10^{-6} $molL^{-1}$), D is the diffusion constant for oxygen in 0.1 **M** KOH (1.9×10^{-5} cm^2s^{-1}) and ν is the kinetic viscosity (0.01 cm^2 s^{-1}). The coefficient 0.2 is used when the rotation speed is expressed in rpm.

The number of transferred electrons (n) and J_k can be find out from slope and intercept of Koutecky–Levich plots, respectively. The value of total electron transfer (n) and percentage of HO_2^{-1} production for RRDE can be calculated as follows.

$$n = \frac{4i_{disk}}{i_{disk} + \frac{i_{ring}}{N}}$$

$$HO_2^- \% = \frac{200i_{disk}}{N(i_{disk} + \frac{i_{ring}}{N})} \times 100$$

The potential difference between Pt ring and GCE disk was maintained 1.5V. The I_{disk} and I_{ring} are the values of the current for disk and ring respectively. *N* is the current collection efficiency, which was found to be 0.37.

The low energy gap between LUMO and HOMO provide the information about the reactivity of the complex molecule.

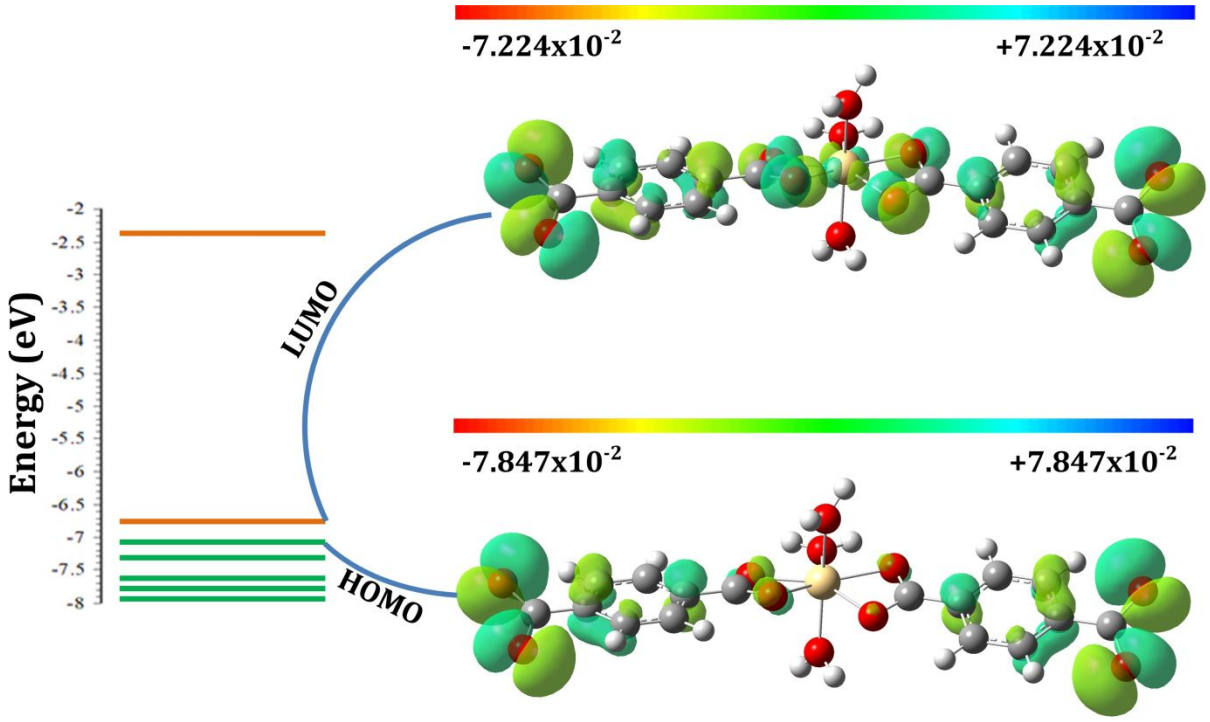

Figure S1. A section of molecular orbital energy diagram for Cd-MOF.

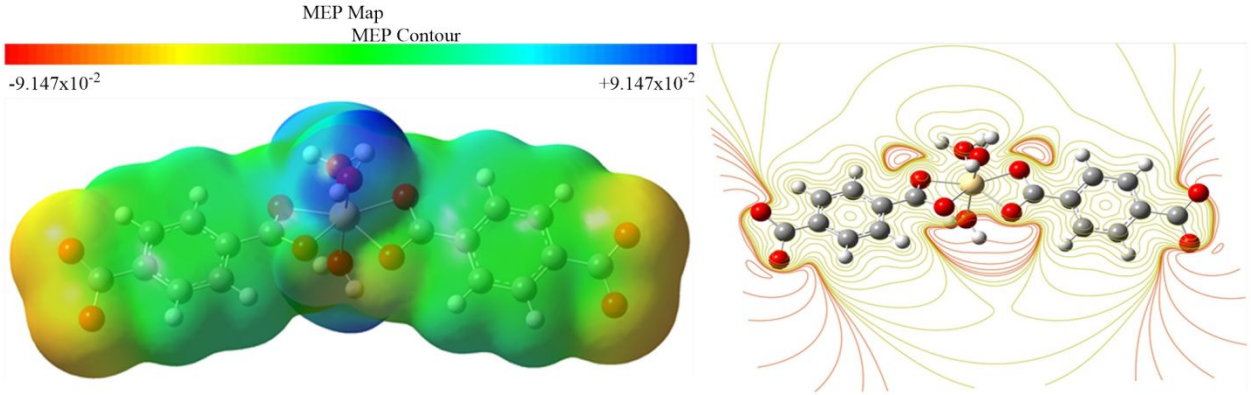

Figure S2. MEP map and contour diagram of molecular orbitals for Cd-MOF.

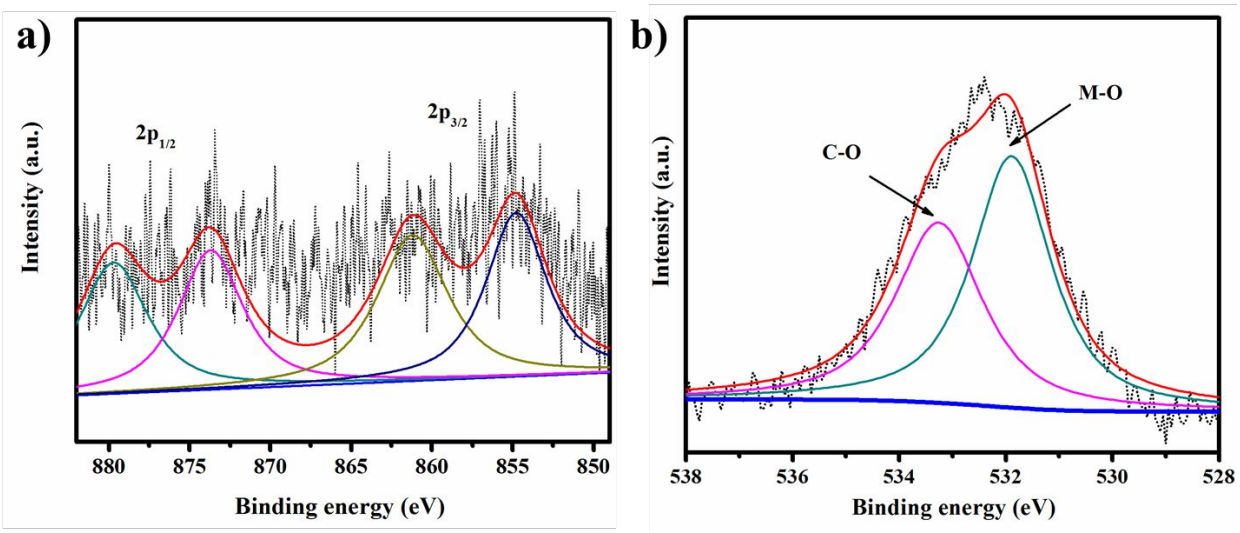

Figure S3. XPS spectra (a) Ni2p core line of Pt-Ni@PC900 and (b) O1s core line of Pt-Ni@PC900.

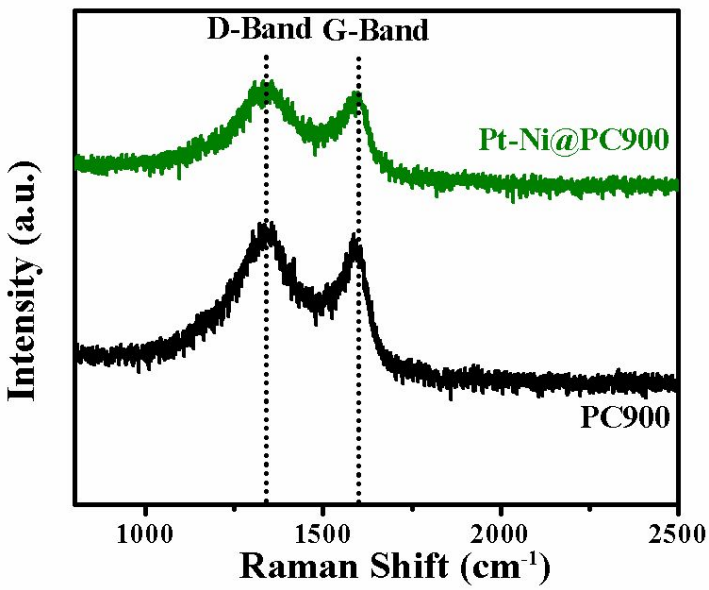

Figure S4. Raman spectra of PC900 and Pt-Ni@PC900**.**

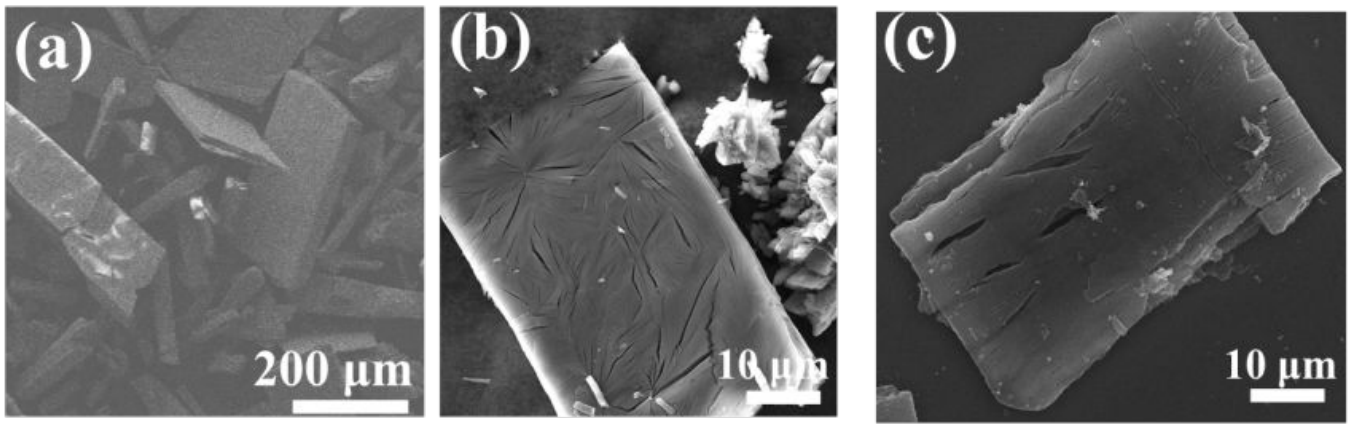

Figure S5. SEM images (a) Cd-MOF, (b) PC900 and (c) Pt-Ni@PC900.

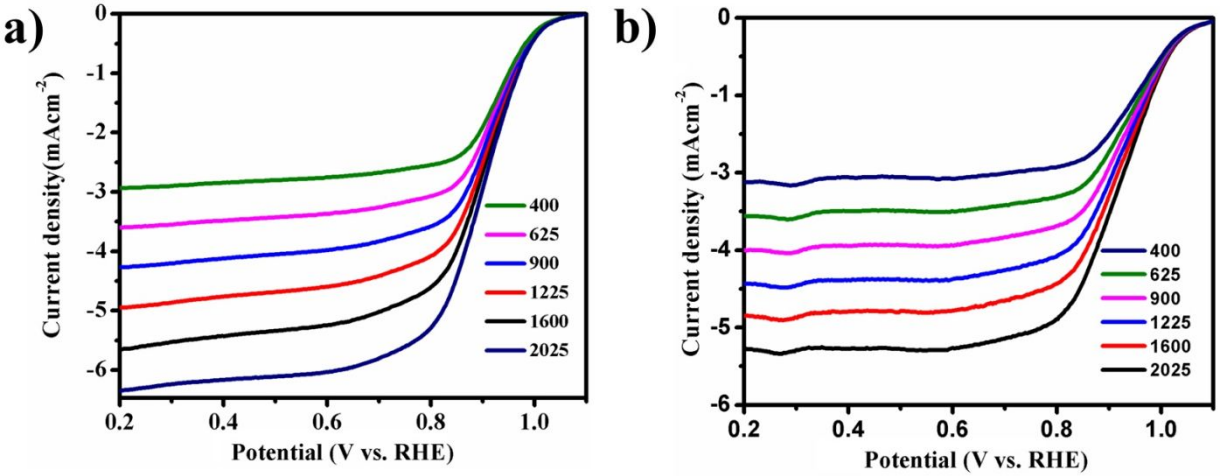

Figure S6. Results of LSV curves for ORR on RDE with varying speed of rotation from 400-2025 rpm in 0.1 M KOH at 5 mV s^{-1} scan rate, (a) Pt-Ni@PC900 and (b) 20%Pt/C.

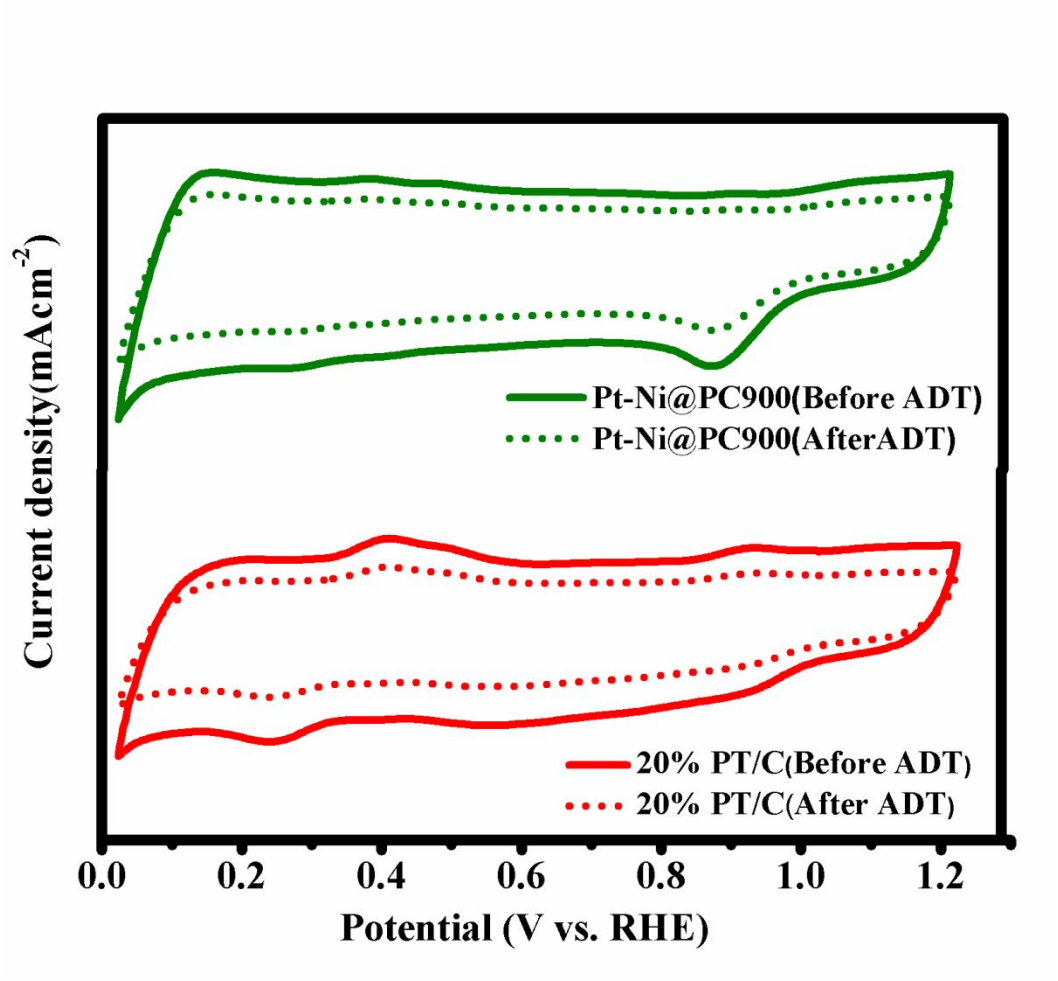

Figure S7. CV curves on RDE for Pt-Ni@PC900 and 20%Pt/C electrode (catalyst loading amount: 316 µg cm^{-2}) at 50 mVS^{-1} in O_2-saturated 0.1 M KOH (solid line represents before ADT and dotted line represents after ADT).

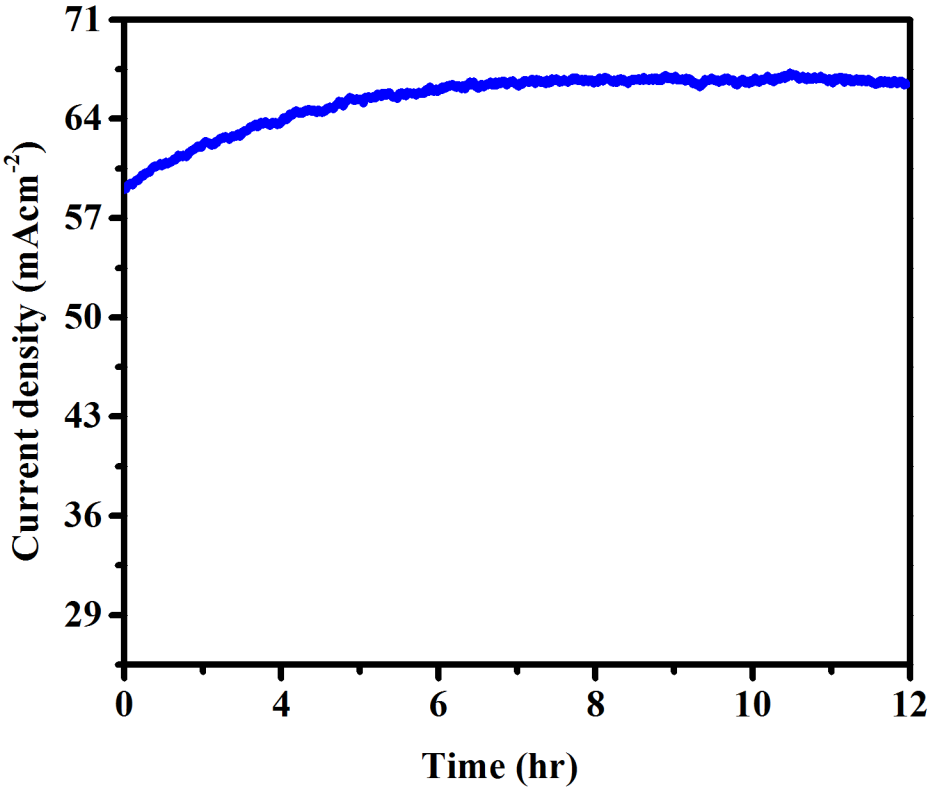

Figure S8.Durability test of Pt-Ni@PC900 in 1 **M** KOH solution (time-dependent current density curve under constant potential of 0.5 V versus Ag/AgCl).

Table S1. Crystal data and structure refinement details of $[C_8H_{10}CdO_7]_n.4H_2O$

Parameters	Cd-MOF
Empirical formula	$[C_8H_{18}CdO11$
Formula weight	402.62
T (K)	130(2) K
Wavelength (Å)	0.71073
Crystal system	Orthorhombic
Space group	Pcca
a (Å)	7.2226(9)
b (Å)	9.9625(12)
c (Å)	19.800(2)
α (°)	90
β (°)	90
γ (°)	90
Volume ($Å^3$)	1424.71(30)
Z	4
D calc (Mg/m^3)	1.877
Absorption coefficient(mm^{-1})	1.584
F(000)	808
Crystal size (mm^3)	0.470x 0.100 x 0.090
θ(°) range	2.04 to 27.88
Reflections collected	7204
Limiting indices	$-9\leq h\leq 8$, $-12\leq k\leq 12$, $-24\leq I\leq 21$
R(int)	0.0339
Completeness to θ = 27.88°	99.90%
CCDC No.	1503652

Table S2. Theoretical structural parameters of Cd-MOF at B3LYP/LANL2DZ level.

Bond Lengths (Å)					
	DFT	EXP.		DFT	EXP.
Cd1-O1	2.057	2.357	Cd1-O9	2.050	2.250
Cd1-O2	2.061	2.500	Cd1-O10	2.045	2.250
Cd1-O7	2.046	2.357	Cd1-O11	2.041	2.236
Cd1-O8	2.049	2.500	-	-	
Bond Angles (º)					
	DFT	EXP.		DFT	EXP.
O1-Cd1-O2	63.6	53.79	O7-Cd1-O8	63.9	53.79
O1-Cd1-O7	146.0	140.89	O7-Cd1-O9	98.6	91.48
O1-Cd1-O8	87.2	87.10	O7-Cd1-O10	85.1	84.8
O1-Cd1-O9	92.4	89.85	O7-Cd1-O11	74.7	68.9
O1-Cd1-O10	78.7	82.66	O8-Cd1-O9	78.8	78.2
O1-Cd1-O11	136.5	136.45	O8-Cd1-O10	93.1	92.9
O2-Cd1-O7	149.0	140.89	O8-Cd1-O11	136.2	137.1
O2-Cd1-O8	146.2	140.89	O9-Cd1-O10	168.3	165.32
O2-Cd1-O9	85.5	84.8	O9-Cd1-O11	94.7	89.85
O2-Cd1-O10	97.0	93.5	O10-Cd1-O11	97.0	95.9
O2-Cd1-O11	74.3	73.9	-	-	
Dihedral Angles (º)					
	DFT	EXP.		DFT	EXP.
C7-O1-Cd1-O7	168.1	176.42(16)	C16-O7-Cd1-O1	33.9	-
C7-O1-Cd1-O8	-161.3	-176.61(17)	C16-O8-Cd1-O2	-169.1	-176.61(17)
C7-O2-Cd1-O7	-167.0	-176.61(17)	C16-O7-Cd1-O1	-160.9	-176.61(17)
C7-O2-Cd1-O8	31.8	-	C16-O8-Cd1-O2	170.0	176.42(16)

Table S3. Reported experimental and their calculated harmonic frequencies (cm^{-1}) at B3LYP/LANL2DZ level in vacuo for Cd-MOF.

Assignments[a]	Frequencies	
	Experimental	Calculated
$\nu_{OHasymmetric}$	3556	3750
$\nu_{OHsymmetric}$	3474	3600
$\nu_{C=O,}$ α_{O-H}	1639	1632
$\nu_{C=C}$	1616	1598
ν_{C-O},ν_{C-C},γ_{C-H}	1410	1430
ω_{O-H}	883	882
ω_{O-H}	736	702
ω_{O-H}, α_{O-H}, ν_{C-C}, ν_{Cd-O}	621,481	643, 487

[a] ν: stretching, α: scissoring, γ: rocking, ω: wagging

Table S4. Elemental analysis result for Pt-Ni@PC900 from XPS, CHNS/O and ICP-OES measurements.

Elements	Atomic % (XPS Analysis)	Atomic % (CHNS/O Analysis)	Wt. % (ICP-OES)
C	80.94	83.23	-
O	10.34	12.38	-
Pt	5.8	-	6.03
Ni	2.92	-	3.73

Table S5. Raman parameters calculated from Raman spectra of PC900 and Pt-Ni@PC900.

	G-Band	I_G	D-Band	I_D	$R=I_D/I_G$
PC900	1584	21.2	1339	22.3	1.052
Pt-Ni@PC900	1600	15.3	1342	15.8	1.027

Table S6. Textural parameters of $[C_8H_{10}CdO_7]_n.4H_2O$, PC900 and Pt-Ni@PC900 obtained from the N_2 adsorption–desorption isotherms.

	Specific surface area ($m^2\ g^{-1}$)	Pore volume ($cm^3\ g^{-1}$)	Mean pore size (nm)
PC900	877.01	1.13	5.1
Pt-Ni@PC900	359.49	0.43	3.5

References

[1] R. Dennington, T. Keith, J. Millam, GaussView, version 5, Semichem Inc., Shawnee Mission, KS, (2009).

[2] M. Frisch, G. Trucks, H. Schlegel, G. Scuseria, M. Robb, J. Cheeseman, G. Scalmani, V. Barone, B. Mennucci, G. Petersson, 09, Revision D. 01, Gaussian, Inc., Wallingford, CT, (2009).

[3] X. Xu, W.A. Goddard, The X3LYP extended density functional for accurate descriptions of nonbond interactions, spin states, and thermochemical properties, Proceedings of the National Academy of Sciences of the United States of America, 101 (2004) 2673-2677.

[4] C. Lee, W. Yang, R.G. Parr, Development of the Colle-Salvetti correlation-energy formula into a functional of the electron density, Phys. Rev. B, 37 (1988) 785.

[5] K. Sayin, N. Kurtoglu, M. Kose, D. Karakas, M. Kurtoglu, Computational and experimental studies of 2-[(E)-hydrazinylidenemethyl]-6-methoxy-4-[(E)-phenyldiazenyl] phenol and its tautomers, J. Mol. Struct., 1119 (2016) 413-422.

[6] H. Keypour, M. Shayesteh, M. Rezaeivala, K. Sayin, Dinuclear Cu (II) complexes of compartmental Schiff base ligands formed from unsymmetrical tripodal amines of varying arm lengths: Crystal structure of [Cu 2 L 1](ClO 4) 2 and theoretical studies, J. Mol. Struct., 1112 (2016) 110-118.

[7] G.M. Sheldrick, A short history of SHELX, Acta Crystallogr. Sect. A: Found. Crystallogr., 64 (2007) 112-122.

[8] M. Nadeem, M.H. Bhatti, K. Sayin, U. Yunus, M. Mehmood, S. Mehboob, U. Flörke, Crystal structure, thermal, luminescent and terahertz time domain spectroscopy of magnesium N-phthaloyl-β-alaninate: A combined experimental and theoretical study, J. Mol. Struct., (2018).

[9] S. Mehboob, M. Mehmood, M. Ahmed, J. Ahmad, M.T. Tanvir, I. Ahmad, Terahertz time domain spectroscopy of hydrothermally synthesized boehmite and ammonium dawsonite nanostructures, Infrared Phys. Technol., 78 (2016) 200-208.